Journal of Thermal Analysis and Calorimetry (2020) 142:1031–1042
https://doi.org/10.1007/s10973-020-09857-8

Sulfation performance of CaO under circulating fluidized bed combustion-like condition

Y. J. Bai[1,2] · M. Q. Chen[1,2] · Q. H. Li[3] · Y. W. Huang[1,2]

Received: 27 August 2019 / Accepted: 16 May 2020 / Published online: 2 June 2020

Abstract

As a major air pollutant, SO_2 has negative effect on the human health and environment. The desulfurization characteristics of two CaO samples (commercial one and the other one calcined from $CaCO_3$) with high purity were examined by a thermo-gravimetric analyzer under circulating fluidized bed combustion-like condition. The influences of SO_2 concentration (1000–4000 ppm), CO_2 concentration (0–45%) and temperatures (800–950 °C) on the sulfation conversion degree of CaO samples were addressed, and sulfation kinetic parameters for the two samples were estimated based on the unreacted shrinking core model. The sulfation conversion degree of CaO calcined from $CaCO_3$ at 900 °C and 2000 ppm SO_2 was 68% higher than the commercial CaO. The sulfation conversion degree for the commercial CaO at 950 °C with 2000 ppm SO_2 was one time higher than at 800 °C, and the sulfation conversion degree for the sample calcined from $CaCO_3$ at 950 °C increased by about 31% compared to that at 800 °C. The calcium conversion degree of the sample calcined from $CaCO_3$ was 0.59 in the absence of CO_2, and the conversion degree with the CO_2 concentration of 45% reduced by about 31%. The sulfation kinetics of two samples were appropriately described by the shrinking unreacted core model. The sample calcined from $CaCO_3$ had a better sulfation activity than the commercial CaO.

Keywords CaO · $CaCO_3$ · SO_2 · Sulfation · Kinetics · Circulating fluidized bed

Abbreviation

b	Stoichiometric coefficient
A, B	Characteristic time in Eqs. (4a) and (4b) (min)
A_1, B_1	Revise factors of time in Eqs. (4a) and (4b) (min)
C_{A0}	SO_2 concentration (mol mL^{-1})
C_{S0}	CaO concentration (mol mL^{-1})
D_0	Pre-exponential factor of the product layer diffusion reaction (cm^2 min^{-1})
D_s	Effective diffusivity of reactants in the product layer (cm^2 min^{-1})
E_a	Activation energy for chemical reaction stage (kJ mol^{-1})
E_p	Activation energy for product layer diffusion (kJ mol^{-1})
$G_{fp}(x)$	Function defined by Eq. (6a)
k	Rate constant of the surface reaction (cm min^{-1})
k_0	Pre-exponential factor of the surface reaction (cm min^{-1})
m	Mass (mg)
M	Molar mass (g mol^{-1})
$P_{fp}(x)$	Function defined by Eq. (6b)
R	General gas constant (J mol^{-1} K^{-1})
R_p	Original radius of the sorbent particle (cm)
t	Time (min)
T	Temperature (K)
W	Mass percentage
x	Conversion degree

Greek letter

δ	Standard uncertainty

Subscript

0	Initial

✉ M. Q. Chen
mqchen@bjtu.edu.cn

✉ Q. H. Li
liqh@tsinghua.edu.cn

[1] Institute of Thermal Engineering, School of Mechanical, Electronic and Control Engineering, Beijing Jiaotong University, Beijing 100044, People's Republic of China

[2] Beijing Key Laboratory of Flow and Heat Transfer of Phase Changing in Micro and Small Scale, Beijing 100044, People's Republic of China

[3] Key Laboratory for Thermal Science and Power Engineering of Ministry of Education, Department of Energy and Power Engineering, Tsinghua University, Beijing 100084, People's Republic of China

Introduction

Coal is the most important energy source in China and will maintain its dominate position in the foreseeable future [1, 2], and the coal combustion would produce a large amount of pollutants [3]. Sulfur dioxide (SO_2), as a common air pollutant around the world, can harm the human health and cause destruction to the environment [4–6]. SO_2 emissions mainly come from coal-fired power plants [7]. In the past decades, many studies have been devoted to reducing SO_2 emission from fossil fuel combustion process [8]. For example, for the flue gas cleaning, many different techniques such as wet scrubbing, dry scrubbing, direct dry sorbent injection and regenerable process have been developed for sulfur capture removal [9]. For fluidized bed combustors (FBCs), capturing SO_2 in situ using a calcium-based sulfur sorbent (calcitic limestone or dolomite) is feasible [10]. Circulating fluidized bed combustion (CFBC) is a promising technology for burning high-sulfur fuels [11–13]. In addition to its fuel flexibility, it has other advantages such as the low NO_x emissions owing to low combustion temperatures and low SO_2 emissions due to the in situ desulfurization using calcium-based sorbents [14–16]. Downstream flue gas desulfurization technology in pulverized coal power plants is usually an alternative to in situ addition. But, compared to in situ sulfur capture in CFBC especially for high-sulfur coals, the downstream flue gas desulfurization would lead to the more complex and costly system [17].

The main way to reduce sulfur oxides produced during fluidized bed combustion (FBC) is to inject calcium-based sorbents (limestone or dolomite) into high-temperature region of the furnace [10]. In the CFBC, the temperature is relatively low, about 850 °C, along with longer residence time of sorbent particles which are beneficial to desulfurization [7, 18].

Limestone as an effective and economic sorbent is widely used for the in situ desulfurization process [9, 19, 20]. For the air-fired fluidized bed, the limestone desulfurization process is divided into two steps: the limestone is calcined into CaO and CO_2; and then, the porous CaO reacts with SO_2 in the presence of O_2 to form $CaSO_4$ at high temperature [21, 22]:

$$CaCO_3(s) \leftrightarrow CaO(s) + CO_2(g) \quad (1)$$

$$CaO(s) + SO_2(g) + \frac{1}{2}O_2(g) \leftrightarrow CaSO_4(s) \quad (2)$$

Moreover, the limestone sulfation has two distinguished stages: a quick reaction stage controlled by chemical reaction and a slow reaction stage with solid-state diffusion [10, 19].

However, the limestone sulfation rate decreases rapidly during the reaction process [23], and the calcium conversion degree in the limestone usually reaches only 30–40% [10]. Therefore, in order to remove sufficient SO_2, it is often necessary to add over-stoichiometric sorbent to the furnace, which would lead to the increased solid waste generation [24]. The rapid decreasing in the sulfation rate can be related to that molar volume of $CaSO_4$ is much higher than CaO, which would give rise to small pores in CaO to be plugged by $CaSO_4$ even a $CaSO_4$ layer covers over CaO grains [25, 26].

The sulfur removal ability of Ca-based sorbents can be influenced by pore structure of sorbents, temperature, SO_2 concentration and CO_2 concentration [9]. For air-fired CFBBs, the optimum desulfurization temperature for calcium-based sorbent is about 850 °C [19, 27, 28]. The effect of the temperature are realized through changing the physical properties of limestone such as the sintering of solid reactant and the pore blockage by $CaSO_4$ product [29, 30], combined with the reductive decomposition of product $CaSO_4$ at high temperature. There is an optimum value existed for the efficiency of SO_2 removal at a certain temperature [19]; then, it decreases with the increase in the bed temperature [31]. The sulfation rate of calcium-based sorbent can be enhanced by the increase in the SO_2 concentration, according to Abanades et al. [19] and de Diego et al. [14] reported.

Pore structure of CaO includes specific surface area, porosity and pore size distribution. Many researchers have examined the effect of pore structure on the sulfation of CaO calcined from calcium-based sorbent (limestone or $Ca(OH)_2$). Gullett and Bruce [32] examined the sulfation behavior of CaO (calcined from limestone containing 95% $CaCO_3$) experiencing different sintering durations and pointed out that although sintering can cause the coalescence of pores less than 7 nm and reduce specific surface area by a half, the sulfation behavior is not influenced significantly, which indicates that the pores smaller than 7 nm are not crucial for the sulfation behavior of CaO. Ghosh-Dastidar et al. [33] noted that the internal pore structure of CaO (calcined from $Ca(OH)_2$) has a determining effect on the initial reactivity and the final utilization of CaO, but a high specific surface area cannot ensure a high sulfation reactivity and conversion degree. If the CaO particles contain an abundance of small pores, the sulfation reaction would cease prematurely because small pores are very susceptible to pore blockage and plugging [23]. Moreover, Mahuli et al. [34] figured out that in order to improve the sulfation performance of CaO (calcined from modified calcium carbonate), the total pore surface and pore volume should be enlarged, but also the proportion of pores in the size range of 5–20 nm should be increased.

Thermo-gravimetric analysis (TGA) is a common used method for studying the sulfation characteristics of Ca-based sorbents, by which reaction kinetic parameters can be obtained [31, 35]. Grain model is usually used to describe the sulfation reaction kinetics for limestone sorbent [36, 37], which is based on the assumption that the porous solid is composed of uniform size, spherically shaped and small non-porous grains [38]. Also, the conversion of each grain can be commonly described by the shrinking unreacted core model that is modified form of the grain model [37]. The shrinking unreacted core model is the most commonly used model for limestone sulfation [39–42], by assuming a clear interface existed between the unreacted core and the product layer during gas–solid reactions of the sorbent particles, and the sulfation reaction occurred from the particle surface to the inner surface [43]. The reaction initiates on the grain surface in so-called chemical reaction-controlled stage. A layer of $CaSO_4$ product is gradually formed around each CaO grain that separates the reaction surface of the solid from gas reactant. The gas molecules have to diffuse through the product layer to the reaction surface, which means that the sulfation reaction shifts to the product layer diffusion-controlled stage [44].

Most of the works focus on the sulfation characteristics of limestone or other industrial materials including dolomite, sodium carbonate and bicarbonate [45], as well as some calcium-based industrial waste such as carbide slag and white mud [46]. Limestone is a complicated material with many impurities such as MgO, SiO_2 and Fe_2O_3, which would lead to high uncertainty and disagreement in the literature on the sulfation performance due to different limestone sources [47]. The sulfation performances and kinetics for commercial CaO and CaO calcined from $CaCO_3$ with high purity as CFBC in situ desulfurization sorbents are rarely reported. In addition, the effect of CO_2 concentration on sulfation characteristics of CaO calcined from $CaCO_3$ at circulating fluidized bed conditions is not still seen.

In this work, the sulfation conversion and kinetics of reagent-grade commercial CaO and CaO calcined from $CaCO_3$ are studied based on a thermo-gravimetric analysis technique. The effects of temperature, SO_2 concentration and CO_2 concentration on the sulfation characteristics of two CaO samples are examined. The kinetic parameters based on the unreacted shrinking core model are estimated. The data would provide a basic reference for well understanding the sulfation characteristics of reagent-grade CaO samples and developing sorbents with high sulfation performance.

Methods

Materials

Reagent-grade calcium oxide (CaO) and calcium carbonate ($CaCO_3$) were purchased from a biochemical technology company (Macklin, Shanghai, China). The chemical compositions of commercial CaO, $CaCO_3$ as well as CaO calcined from $CaCO_3$ were analyzed by a X-ray fluorescence spectrometer (XRF-1800, SHIMADZU, Japan), which are listed in Table 1.

Experimental

The desulfurization reaction processes of CaO calcined from $CaCO_3$ and commercial CaO were tested through a thermo-gravimetric analyzer (ZCT-A, JINGYIGAOKE, China) in simulated fuel gas. TGA was carried out with four electronic mass flow controllers (HXMF02, HUAXUSHIJI, China) to supply a synthetic flue gas mixture consisting of SO_2, CO_2, O_2 and N_2. The gas mixture is composed of SO_2, CO_2, O_2 and N_2 from gas cylinders, and the each concentration was adjusted by a mass flow controller.

In CFBCs, the flue gases usually consist of about 15% CO_2, 3–5% O_2, 5–15% H_2O, small amounts of SO_x, NO_x and balance N_2 [48], and the typical bed temperatures are between 800 and 950 °C [10]. The simulated flue gas compositions and experimental temperatures are listed in Table 2. The initial mass of sample is 5 ± 0.5 mg, and the total flow rate of the synthesis gas was set as 100 mL min^{-1}.

Before synthetic flue gas was injected, commercial CaO sample was calcined at 800 °C in N_2 for 10 min in order to remove any residual carbonate or hydroxide species and to ensure that the pure calcium oxide is the only metal species [49]. After the calcination pre-treatment, commercial CaO sample was heated from room temperature to setting temperature with a heating rate of 20 K min^{-1} at the presence of CO_2, O_2 and N_2, which was kept about five minutes to ensure the temperature stabilization. SO_2 was introduced into the synthetic flue gas to start the sulfation reaction. The test duration was set as 5 h [17]. After 5 h, the system was purged with N_2

Table 1 Chemical composition of commercial CaO, $CaCO_3$ and CaO calcined from $CaCO_3$ (mass%)

Samples	$CaCO_3$	CaO	SiO_2	MgO	Al_2O_3	Fe_2O_3	Na_2O	K_2O	SO_3	Others
Commercial CaO		98.47	0.229	0.495	0.157	0.0919	0.291	0.0182	0.108	0.1699
CaO calcined from $CaCO_3$		99.35	0.0446	0.0278	0.0129	0.0052	0.305	–	0.170	0.0845
$CaCO_3$	99.51	–	–	0.05	–	0.005	0.1	0.005	0.01	–

Table 2 Experimental conditions

T/K	CO_2 concentration/%	O_2 concentration/%	SO_2 concentration/ppm	N_2/%	Particle size/μm
1073, 1123, 1173, 1223	0, 15, 45	5	1000, 2000, 3000, 4000	Balance	106–250

for 2 h to make TGA facility cool down to the room temperature before the sample was removed out. For CaO calcined from $CaCO_3$, after the reaction chamber was heated to 900 °C, the chamber is kept at the same temperature for ten minutes, in order to ensure temperature stabilization and completion of the calcination [45]. After that, the temperature was adjusted to desired setting temperatures, and SO_2 was injected into the gas to start the sulfation experiment.

For CO_2 concentration of 45%, the reaction temperature was only kept at 900 °C (1173 K).

The measurement parameter uncertainties are calculated as follows:

$$\text{The uncertainty of mass: } \pm\frac{\delta m}{m}=\pm\frac{0.001/2\sqrt{3}}{5}=\pm 0.006\%$$

$$\text{The uncertainty of temperature: } \pm\frac{\delta T}{T}=\frac{0.01\Big/2\sqrt{3}}{25}=\pm 0.1\%$$

where m is the sample mass, mg; T the initial experimental temperature, °C; δm the standard uncertainty of mass, mg; and δT the standard uncertainty of temperature, °C.

The experiments for commercial CaO at 850 °C, 1000 ppm and 2000 ppm SO_2, as well as for CaO calcined from $CaCO_3$ at 2000 ppm SO_2, 900 °C and 950 °C were repeated three times, respectively, as illustrated in Fig. 1.

The relative deviations in the chemical reaction-controlled stages for two samples were less than ± 3%, indicating that there is a good reproducibility for the tests.

Sulfation conversion degree

The sulfation conversion degree of Ca-based sorbents can be calculated by [50]:

$$x=\frac{\Delta m M_{\mathrm{CaO}}}{m_0 W_{\mathrm{CaO}}\left(M_{\mathrm{CaSO_4}}-M_{\mathrm{CaO}}\right)} \tag{3}$$

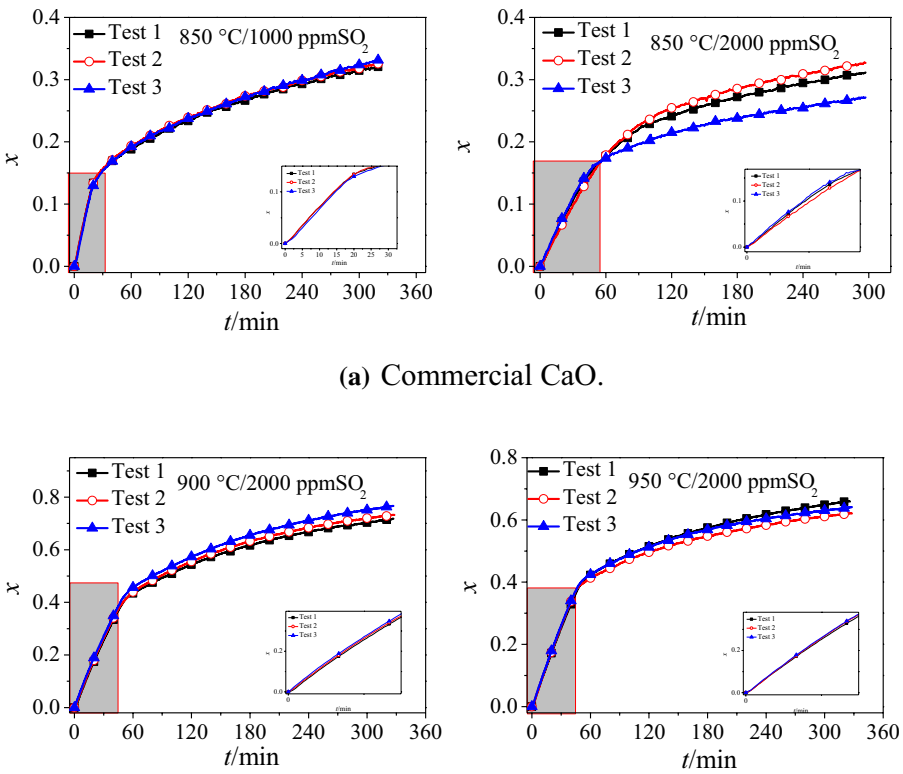

Fig. 1 Repetitive experiments

(a) Commercial CaO.

(b) CaO calcined from $CaCO_3$.

where m_0 is the initial mass of sorbents, mg; Δm the mass added after SO_2 adsorption reaction, mg; M_{CaO} the molar mass of CaO, g mol^{-1}; M_{CaSO4} the molar mass of $CaSO_4$, g mol^{-1}; and W_{CaO} the mass percentage of CaO in the sorbent.

Sulfation kinetics

The sulfation of Ca-based is a non-catalyst gas–solid reaction [51], and the unreacted shrinking core model is usually used in describing the sulfation reaction between calcium-based sorbent and SO_2 [42, 44, 46, 50–53], which can be written as:

$$t = A_1 + AG_{fp}(x) \tag{4a}$$

for chemical reaction-controlled process, and

$$t = B_1 + BP_{fp}(x) \tag{4b}$$

for product layer diffusion-controlled process, where t is the reaction time, min; A_1 and B_1 the revise factors of time, min; x the calcium conversion degree of sorbent; $G_{fp}(x)$ the function of calcium conversion degree during chemical reaction-controlled stage; and $P_{fp}(x)$ the function of calcium conversion during product layer diffusion-controlled stage; and A and B are the characteristic times, min, which can be given by

$$A = \frac{C_{S0}R_P}{kC_{A0}} \tag{5a}$$

$$B = \frac{C_{S0}R_P^2}{6bD_sC_{A0}} \tag{5b}$$

$$G_{fp}(x) = 1 - (1-x)^{1/3} \tag{6a}$$

$$P_{fp}(x) = 1 - 3(1-x)^{2/3} + 2(1-x) \tag{6b}$$

where C_{A0} is the concentration of SO_2 in the fuel gas, mol mL^{-1}; C_{S0} the concentration of CaO in the sorbent, mol mL^{-1}; R_p the original radius of the sorbent particle, cm; b the stoichiometric coefficient of the reaction, $b = 1$; k the rate constant of the surface reaction, cm min^{-1}; and D_s the effective diffusivity of reactant in the product layer, cm^2 min^{-1}.

The value of $1/A$ can be obtained by plotting $G_{fp}(x)$ versus t, and the value of $1/B$ can be obtained by plotting $P_{fp}(x)$ versus t. The logarithms of Eqs. (5a) and (5b) can be expressed as:

$$\ln k = \ln(1/A) + \ln\left(R_pC_{S0}/C_{A0}\right) \tag{7a}$$

$$\ln D_s = \ln(1/B) + \ln\left(R_p^2C_{S0}/6bC_{A0}\right) \tag{7b}$$

According to the Arrhenius equation:

$$k = k_0e^{-E_a/RT} \tag{8a}$$

for chemical reaction-controlled process, and

$$D_s = D_0e^{-E_p/RT} \tag{8b}$$

for product layer diffusion-controlled process, where k_0 is the pre-exponential factor of the surface reaction, cm min^{-1}; E_a the activation energy for surface chemical reaction, kJ mol^{-1}; D_0 the pre-exponential factor of the product layer diffusion reaction, cm^2 min^{-1}; E_p the activation energy for product layer diffusion, kJ mol^{-1}; R the general gas constant, 8.314 J mol^{-1} K^{-1}; and T the temperature, K.

From Eqs. (7a) and (8a), a relationship between $1/A$ and $1/T$ can be described as

$$\ln(1/A) = -E_a/RT + \ln k_0 - \ln\left(R_pC_{S0}/bC_{A0}\right) \tag{9a}$$

From Eqs. (7b) and (8b), a relationship between $1/B$ and $1/T$ can be described as

$$\ln(1/B) = -E_p/RT + \ln D_0 - \ln\left(R_p^2C_{S0}/6bC_{A0}\right) \tag{9b}$$

The values of E_a and k_0 can be estimated by plotting $\ln(1/A)$ versus $1/T$, and the values of E_p and D_0 can be estimated by plotting $\ln(1/B)$ versus $1/T$.

Results and discussion

Specific surface area, pore volume and pore diameter are important physical properties of solids in reactions, which would influence the Ca utilization of the sorbents [22, 54]. The specific surface area, pore volume and pore diameter of the commercial CaO, $CaCO_3$ and CaO calcined from $CaCO_3$ were determined using a surface area and porosity analyzer (ASAP 2460, Micromeritics, America) according to BET (Brunner–Emmett–Teller) and BJH (Barrett–Joyner–Halenda) methods, which are summarized in Table 3.

The pore size distribution of commercial CaO, $CaCO_3$ and CaO calcined from $CaCO_3$ is depicted in Fig. 2.

Specific surface area means the region where reactions can occur, while pore volume suggests the space in which the products can grow. Pore diameter is the space limitation in a single pore [54]. Manvoic et al. [22] noted that the high specific surface area is formed mainly from more small pores existed, which is important for the initial chemical reaction-controlled stage. As given in Table 3, the specific surface area of CaO calcined from $CaCO_3$ is almost two times higher than the commercial CaO. From Fig. 2, the pore size of $CaCO_3$ is mainly distributed in 2–4 nm, while that of CaO calcined from $CaCO_3$ is mainly distributed in 20–40 nm, which could be linked to that

Table 3 Physical analysis of two CaO samples and $CaCO_3$

Samples	Specific surface area/ $m^2\ g^{-1}$	Pore volume/ $cm^3\ g^{-1}$	Pore diameter/nm
Commercial CaO	3.98	0.011	13.6
$CaCO_3$	2.23	0.003	7.24
CaO calcined from $CaCO_3$	11.13	0.110	39.52

CO_2 by the decomposition of $CaCO_3$ escapes from the solid. There are two peaks (3–4 nm, 7–10 nm) for the pore size distribution of commercial CaO, and the mean pore size and cumulative pore volume are smaller that of CaO calcined from $CaCO_3$. Just as given in Table 3, pore diameter of CaO calcined from $CaCO_3$ is almost two times higher than the commercial CaO, and pore volume of CaO calcined from $CaCO_3$ is almost nine times more than the commercial CaO. With a larger pore volume, reaction of CaO calcined from $CaCO_3$ will become less limited by the product growing space than the commercial CaO. As a result, the sulfation reaction of CaO calcined from $CaCO_3$ in the second stage controlled by diffusion would be faster, which can be a greater contribution to the final conversion. Large pores formed means that sorbents are not easy to be plugged and provide more space for $CaSO_4$ [22].

Sulfation conversion degree

The changes of the sulfation conversion degree for commercial CaO and CaO calcined from $CaCO_3$ with SO_2 concentration at 850 °C are presented in Fig. 3.

As shown in Fig. 3, with the increasing SO_2 concentration, the sulfation rate and final conversion degree rise for both commercial CaO and CaO calcined from $CaCO_3$. As SO_2 concentration increases from 1000 to 4000 ppm, the sulfation conversion degree of commercial CaO rises by about 37% (from 0.27 to 0.37). As SO_2 concentration degree increases from 1000 to 4000 ppm, the sulfation conversion degree of CaO calcined from $CaCO_3$ enhances by about 58% (from 0.53 to 0.84). Abanades et al. [19] also noted the similar trend about SO_2 effect on the sulfation conversion degree for a kind of limestone with the $CaCO_3$ concentration of 97.1%.

The reaction rate is proportional to SO_2 concentration with a power between 0 and around 1 [11], which means that the sulfation reaction is improved at higher SO_2 concentration [31]. The chemical reaction of the gas–solid reactants is completed through the adsorption of SO_2 at active sites on the solid surface followed by the formation of sulfite ions (SO_3^{2-}) that is further oxidized into sulfate ions [55]. Therefore, the higher SO_2 concentration means the more SO_2 molecules can be adsorbed at the surface of the solid reactant, which would cause more $CaSO_4$ product formed.

Moreover, at a certain SO_2 concentration, CaO calcined from $CaCO_3$ displays higher sulfation conversion degree

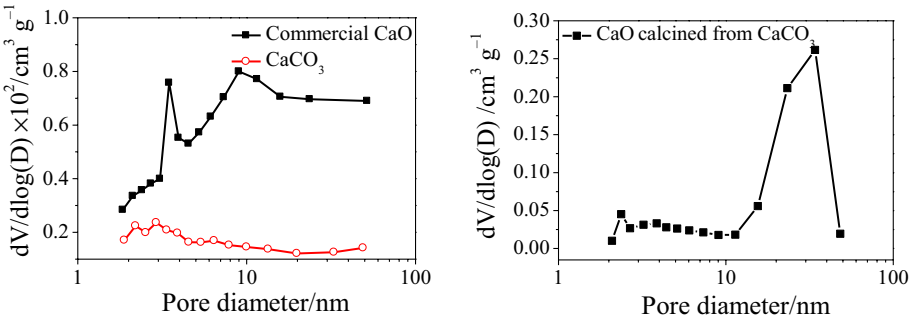

Fig. 2 Pore size distribution of commercial CaO, $CaCO_3$ and CaO calcined from $CaCO_3$

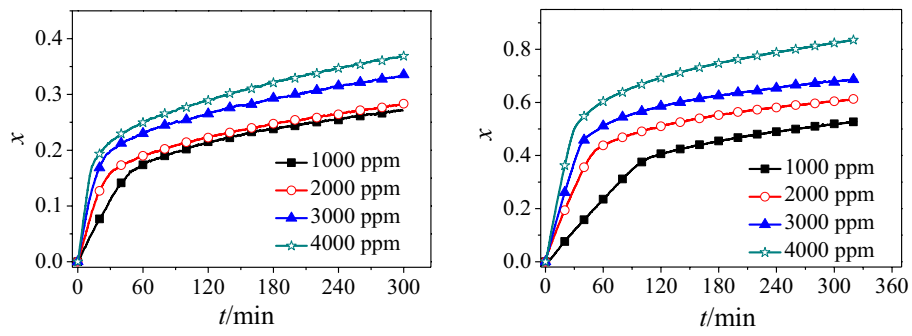

Fig. 3 Changes of the sulfation conversion degree for two CaO samples with SO_2 concentration (15% CO_2; 850 °C; 0.1–0.25 mm)

(a) Commercial CaO. **(b)** CaO calcined from $CaCO_3$.

than commercial CaO, because the CaO calcined from $CaCO_3$ is more reactive and has higher specific surface area than commercial CaO. Between SO_2 concentrations of 1000 and 4000 ppm, the sulfation conversion degree of CaO calcined from $CaCO_3$ is one time higher than commercial CaO.

The changes of the sulfation conversion degree for two CaO samples with temperatures for 2000 ppm SO_2 are depicted in Fig. 4.

From Fig. 4, as the reaction temperature increases, the sulfation rate and ultimate conversion degree of two CaO samples rise. The sulfation conversion degree for the commercial CaO at 950 °C is 0.45, which is one time higher than at 800 °C. The sulfation reaction rate in the initial stage increases with increasing temperature between 800 and 850 °C, which could be related to that thin product layer formed at low temperature is not enough to block the pores. However, the reaction rates over 850 °C for commercial CaO change slightly, which could be linked to the fact that thick product layer formed at high temperature, which is mainly controlled by diffusion through the particles [9]. And for the CaO calcined from $CaCO_3$, within 800–950 °C, the sulfation reaction rate for initial stages (within 1 h) is almost independent on temperature, which can be related to thick product layer formed from its strong activity, indicating that the turning point temperature should be less than 800 °C. García-Labiano et al. [9] identified that the turning point temperature for limestone (97% $CaCO_3$) is about 700 °C.

The sulfation conversion degree for the CaO calcined from $CaCO_3$ at 950 °C increases by about 31% compared to that (0.55) at 800 °C. Yang et al. [7] and Chen et al. [56] proposed that the decomposition rate of $CaCO_3$ increases with the rising of temperature, and the nascent CaO subgrains formed leads to the more specific surface area. Moreover, the high temperature can enhance the chemical reaction rate [57] and reduce the resistance of solid-state diffusion, which would accelerate the diffusion of product layer [51, 58]. Shih et al. [4] and Cheng et al. [59] noted that the product layer formed at higher temperature is more porous.

There is an optimum temperature for SO_2 capture sorbent [21, 31], and the sinterization of sorbent occurs as the sulfation temperature exceeds the optimum temperature [9], which would reduce the surface area and pore volume. In this work, the optimum sulfation temperature for two CaO samples should be around 950 °C, which can be due to the fact that the two samples possess high sinterization resistance due to low alkali metal ion content [51]. Shih et al. [4] and Yang et al. [7] stated that the sulfation conversions of CaO samples calcined from $Ca(OH)_2$ or $CaCO_3$ at 950 °C reach the maximum value. Bragança and Castellan [27] examined the sulfation of a kind of limestone (0.14% Na_2O and 0.74% K_2O) and noted that the optimum temperature is 850 °C. At a certain temperature, CaO calcined from $CaCO_3$ displays higher sulfation conversion than the commercial CaO, which indicate that CaO calcined from $CaCO_3$ possesses better SO_2 capturing capacity than the commercial CaO. For example, the sulfation conversion degree of CaO calcined from $CaCO_3$ at 900 °C is 68% higher than the commercial CaO.

At 2000 ppm SO_2 and 900 °C, the changes of the sulfation conversion degree for CaO calcined from $CaCO_3$ with CO_2 concentration are shown in Fig. 5.

From Fig. 5, both the initial sulfation rate and ultimate conversion degree of CaO calcined from $CaCO_3$ rise with the decreasing in the CO_2 concentration. The calcium conversion degree of CaO calcined from $CaCO_3$ is 0.59 in the absence of CO_2, and the conversion degree with the CO_2 concentration of 45% reduces by about 31%. For this reason, $CaCO_3$ decomposition occurs at higher temperature as the CO_2 concentration increases [35], which means that the presence of CO_2 would result in the delay of $CaCO_3$ decomposition [60]. In addition, CO_2 can enforce the sintering of CaO [7, 38]. Although $CaCO_3$ can react with SO_2 directly, its specific area and pore volume are lower than the formed CaO, which would lead to its low reactivity. At high temperature, CaO particles would coalesce with each other to form denser ones. The coalescence degree of CaO would

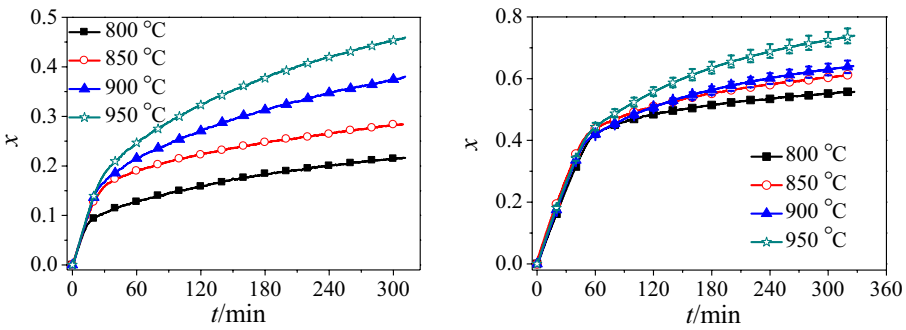

(a) Commercial CaO. **(b)** CaO calcined from $CaCO_3$.

Fig. 4 Changes of the sulfation conversion degree for two CaO samples with temperature. (15% CO_2; 2000 ppm SO_2; 0.1–0.25 mm)

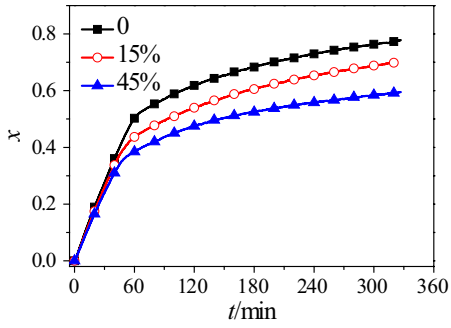

Fig. 5 Changes of the sulfation conversion degree for CaO calcined from $CaCO_3$ with CO_2 concentration (2000 ppm SO_2; 900 °C, 0.1–0.25 mm)

increase with increasing CO_2 concentration, leading to the decrease in the specific surface area and pore volume [7].

Kinetic parameters

According to Eq. (4a), fitting curves of $G_{fp}(x) - t$ for two CaO samples at 2000 ppm SO_2 are shown in Fig. 6, and the slopes of the $G_{fp}(x) - t$, $1/A$ values are determined.

As shown in Fig. 6, $G_{fp}(x)$ with t for the sulfation reaction of the two CaO samples shows linear relationship. For the commercial CaO, the correlation coefficients range from 0.997 to 0.999, while those for the CaO calcined from $CaCO_3$ are 0.999.

According to Eq. (4b), fitting curves of $P_{fp}(x) - t$ for two CaO samples at 2000 ppm SO_2 are presented in Fig. 7, and the slopes of the $P_{fp}(x) - t$, $1/B$ values are estimated.

As shown in Fig. 7, $P_{fp}(x)$ with t for the sulfation reaction of two CaO samples shows linear relationship. For the commercial CaO, the correlation coefficients of $P_{fp}(x) - t$ are between 0.995 and 0.998, while those for the CaO calcined from $CaCO_3$ are between 0.992 and 0.996.

From Figs. 6 and 7, the shrinking unreacted core model is appropriate to describe the sulfation kinetics of two CaO samples.

According to Eq. (9a), fitting curves of $\ln(1/A) - 1/T$ for two CaO samples are shown in Fig. 8.

From the linear fits of $\ln(1/A) - 1/T$ in Fig. 8, the activation energy (E_a) and the pre-exponential factor (k_0) for the surface reaction for two CaO samples are determined, as given in Table 4.

According to Eq. (9b), fitting curves of $\ln(1/B) - 1/T$ for two CaO samples are presented in Fig. 9.

From Fig. 9, the activation energy (E_p) and the pre-exponential factor (D_0) of product layer diffusion reaction for two CaO samples are calculated, which are listed in Table 4.

From Table 4, for two CaO samples, the activation energies in the product layer diffusion (E_p) are always greater than activation energies of the surface reaction (E_a),

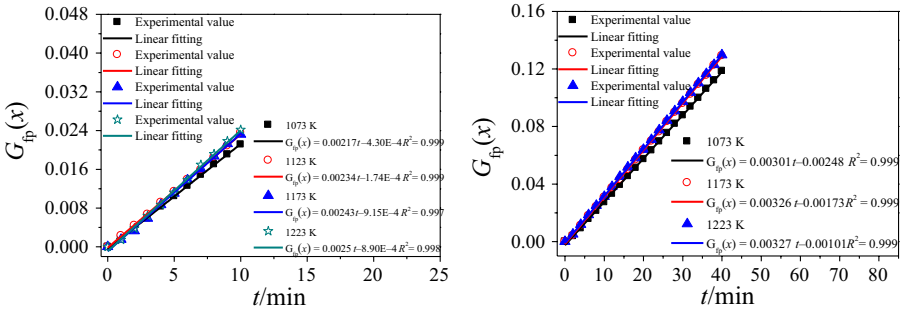

Fig. 6 $G_{fp}(x)$ versus time for two CaO samples

(a) Commercial CaO. **(b)** CaO calcined from $CaCO_3$.

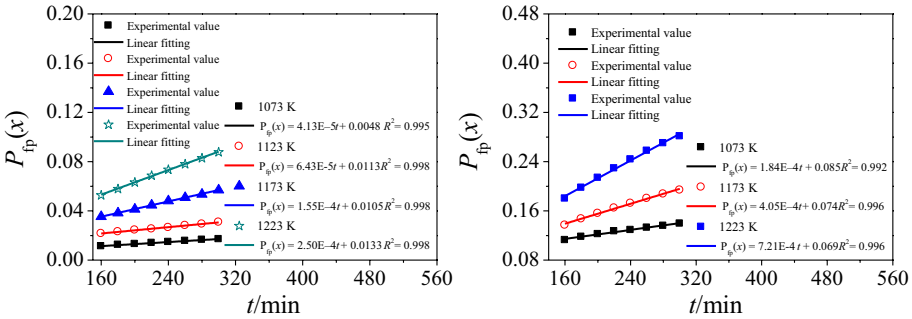

Fig. 7 $P_{fp}(x)$ versus time for two CaO samples

(a) Commercial CaO. **(b)** CaO calcined from $CaCO_3$.

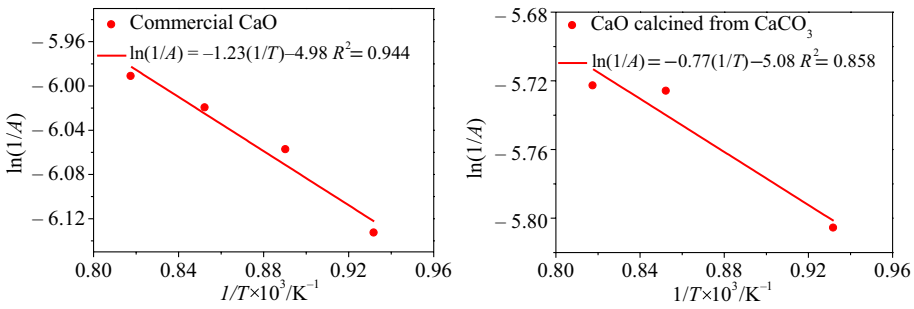

Fig. 8 $\ln(1/A) - 1/T$ fitting curves for two CaO samples

Table 4 Kinetic parameters for two CaO samples

Samples	E_a/kJ mol^{-1}	k_0/cm min^{-1}	E_p/kJ mol^{-1}	D_0/cm^2 min^{-1}
Commercial CaO	10.17	39.47	136.77	1487.37
CaO calcined from $CaCO_3$	6.43	35.76	96.62	76.62

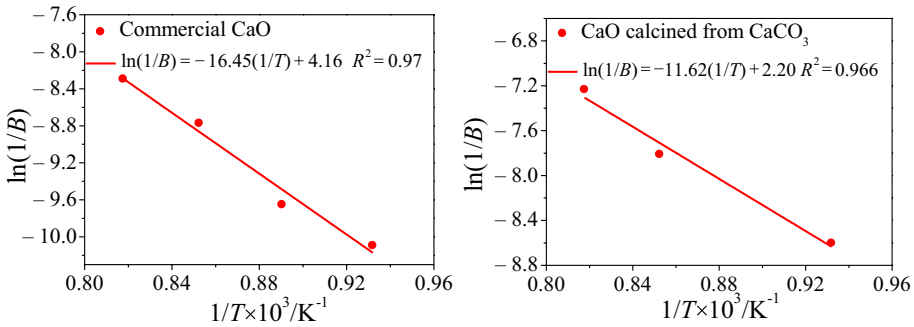

Fig. 9 $\ln(1/B) - 1/T$ fitting curves for two CaO samples

indicating that the diffusion through the product layer is much more difficult than the chemical reaction, which means that the diffusion has a critical influence on the sulfation [52]. Han et al. [51] estimated the activation energies of limestone between the temperatures of 800–1000 °C, which is 19.5 kJ mol^{-1} for E_a and 59.8 kJ mol^{-1} for E_p. Jeong et al. [50] also evaluated the activation energies of limestone between the temperatures of 700–850 °C and identified that the value of E_a is 25.75 kJ mol^{-1}, while the value of E_p is 73.13 kJ mol^{-1}. The values of E_a and E_p for the CaO calcined from $CaCO_3$ in this work are relatively smaller, which can be related to the fact that there is less impurity in the $CaCO_3$.

The values of k_0 and E_a for the sulfation reaction of CaO calcined from $CaCO_3$ are less than the commercial CaO in the chemical reaction controlled stage as well as smaller values of D_0 and E_p in the product layer diffusion stage. However, the activity of sorbent cannot be exactly evaluated only by activation energy because of the compensation effect between the activation energy and the pre-exponential factor in Arrhenius equation [51]. The values of k and D_s can further explain the sulfation reaction [53].

k and D_s for two CaO samples at different temperatures are obtained according to Eqs. (8a) and (8b), as given in Table 5.

Table 5 k and D_s values for two CaO samples

Samples	T/K	k/cm min^{-1}	$D_s \times 10^3$/cm^2 min^{-1}
Commercial CaO	1073	12.80	0.33
	1173	14.09	1.21
	1223	14.69	2.14
CaO calcined from $CaCO_3$	1073	17.39	1.52
	1173	18.50	3.82
	1223	19.00	5.72

Li et al. [46] noted that a larger k value means a better sulfation activity, and a larger D_s indicates higher SO_2 diffusion and calcium cation diffusion capacity through product layer. From the above results, the k value for CaO calcined from $CaCO_3$ is higher than that for the commercial CaO, which means that CaO calcined from $CaCO_3$ possesses a better sulfation activity than the commercial CaO in the chemical reaction-controlled stage. D_s for CaO calcined from $CaCO_3$ is larger than that for the commercial CaO in the product layer diffusion stage. Therefore, CaO calcined from $CaCO_3$ holds higher SO_2 diffusion and calcium cation diffusion

capacity through $CaSO_4$ product layer than the commercial CaO in the product layer diffusion-controlled stage.

Conclusions

As SO_2 concentration increased from 1000 to 4000 ppm, the sulfation conversion degree of the commercial CaO at 850 °C rose by about 37%, and the sulfation conversion degree of CaO calcined from $CaCO_3$ enhanced by about 58% (from 0.53 to 0.84). The optimum sulfation temperature of two CaO samples should be around 950 °C. CaO calcined from $CaCO_3$ had better SO_2 capture capacity than the commercial CaO due to its higher specific surface area and pore volume. For two samples, the activation energies of the product layer diffusion (E_p) were always greater than activation energies of the surface reaction (E_a). The values of k_0 and E_a for the sulfation reaction of CaO calcined from $CaCO_3$ were less than the commercial CaO in the chemical reaction controlling stage as well as smaller values of D_0 and E_p in the product layer diffusion stage.

Acknowledgements This work was supported by the National Key R&D Program of China (Grant No. 2017YFB0603901).

References

1. Xu Y-L, Zuo N, Bu Y-C, Wang L-Y. Experimental study on the characteristics of oxidation kinetics and heat transfer for coal-field fires under axial compression. J Therm Anal Calorim. 2020;139(1):597–607. https://doi.org/10.1007/s10973-019-08379-2.
2. Xian S, Zhang H, Chai Z, Zhu Z. Release characteristics of gaseous products during CO_2 gasification of char. J Therm Anal Calorim. 2020;140(1):177–87. https://doi.org/10.1007/s10973-019-08704-9.
3. Kaljuvee T, Trikkel A, Kuusik R. Decarbonization of natural lime-containing materials and reactivity of calcined products towards SO_2 and CO_2. J Therm Anal Calorim. 2001;64(3):1229–40. https://doi.org/10.1023/A:1011561500091.
4. Shih SM, Lai JC, Yang CH. Kinetics of the reaction of dense CaO particles with SO_2. Ind Eng Chem Res. 2011;50(22):12409–20. https://doi.org/10.1021/ie2009668.
5. Li W, Xu M, Li S. Calcium sulfation characteristics at high oxygen concentration in a 1MWth pilot scale oxy-fuel circulating fluidized bed. Fuel Process Technol. 2018;171:192–7. https://doi.org/10.1016/j.fuproc.2017.11.005.
6. Zhang H, Xian S, Zhu Z, Guo X. Release behaviors of sulfur-containing pollutants during combustion and gasification of coals by TG-MS. J Therm Anal Calorim. 2020. https://doi.org/10.1007/s10973-019-09251-z.
7. Yang JH, Shih SM, Lin PH. Effect of carbon dioxide on the sulfation of high surface area $CaCO_3$ at high temperatures. Ind Eng Chem Res. 2012;51(6):2553–9. https://doi.org/10.1021/ie202665a.
8. Manovic V, Anthony EJ. Sequential SO_2/CO_2 capture enhanced by steam reactivation of a CaO-based sorbent. Fuel. 2008;87(8):1564–73. https://doi.org/10.1016/j.fuel.2007.08.022.
9. García-Labiano F, Rufas A, de Diego LF, Obras-Loscertales MDL, Gayán P, Abad A, et al. Calcium-based sorbents behaviour during sulphation at oxy-fuel fluidised bed combustion conditions. Fuel. 2011;90(10):3100–8. https://doi.org/10.1016/j.fuel.2011.05.001.
10. Anthony EJ, Granatstein DL. Sulfation phenomena in fluidized bed combustion systems. Prog Energy Combust Sci. 2001;27(2):215–36. https://doi.org/10.1016/S0360-1285(00)00021-6.
11. Stewart MC, Symonds RT, Manovic V, Macchi A, Anthony EJ. Effects of steam on the sulfation of limestone and NO_x formation in an air- and oxy-fired pilot-scale circulating fluidized bed combustor. Fuel. 2012;92(1):107–15. https://doi.org/10.1016/j.fuel.2011.06.054.
12. Bolea I, Romeo LM, Pallarés D. The role of external heat exchangers in oxy-fuel circulating fluidized bed. Appl Energy. 2012;94:215–23. https://doi.org/10.1016/j.apenergy.2012.01.050.
13. Park K, Lee JM, Kim DW, Lee GH, Kang Y. Characteristics of co-combustion of strongly caking and non-caking coals in a pilot circulating fluidized bed combustor (CFBC). Fuel. 2019;236:1110–6. https://doi.org/10.1016/j.fuel.2018.09.052.
14. de Diego LF, Rufas A, García-Labiano F, Obras-Loscertales MDL, Abad A, Gayán P, et al. Optimum temperature for sulphur retention in fluidised beds working under oxy-fuel combustion conditions. Fuel. 2013;114:106–13. https://doi.org/10.1016/j.fuel.2012.02.064.
15. Zhao J, Li D, Liao S, Wang D, Wang H, Yan P. Influence of mechanical grinding on pozzolanic characteristics of circulating fluidized bed fly ash (CFA) and resulting consequences on hydration and hardening properties of blended cement. J Therm Anal Calorim. 2018;132(3):1459–70. https://doi.org/10.1007/s10973-018-7103-4.
16. Zhao J, Yang G, Wang D, Liao S, Zhai M. The hydration properties of blended cement containing ultrafine fly ash with particle size less than 17 μm from the circulating fluidized bed combustion of coal gangue. J Therm Anal Calorim. 2020;139(5):2971–84. https://doi.org/10.1007/s10973-019-08685-9.
17. Stewart MC, Manovic V, Anthony EJ, Macchi A. Enhancement of indirect sulphation of limestone by steam addition. Environ Sci Technol. 2010;44(22):8781–6. https://doi.org/10.1021/es1021153.
18. Chen L, Wang C, Wang Z, Anthony EJ. The kinetics and pore structure of sorbents during the simultaneous calcination/sulfation of limestone in CFB. Fuel. 2017;208:203–13. https://doi.org/10.1016/j.fuel.2017.07.018.
19. Abanades JC, de Diego LF, García-Labiano F, Adánez J. Residual activity of sorbent particles with a long residence time in a CFBC. AIChE J. 2000;46(9):1888–93. https://doi.org/10.1002/aic.690460916.
20. Li W, Li S, Xu M, Wang X. Study on the limestone sulfation behavior under oxy-fuel circulating fluidized bed combustion condition. J Energy Inst. 2018;91(3):358–68. https://doi.org/10.1016/j.joei.2017.02.005.
21. Wang C, Jia L, Tan Y, Anthony EJ. The effect of water on the sulphation of limestone. Fuel. 2010;89(9):2628–32. https://doi.org/10.1016/j.fuel.2010.04.022.
22. Manovic V, Anthony EJ, Loncarevic D. SO_2 retention by CaO-based sorbent spent in CO_2 looping cycles. Ind Eng Chem Res. 2009;48(14):6627–32. https://doi.org/10.1021/ie9002365.
23. Han R, Sun F, Gao J, Wei S, Su Y, Qin Y. Trace Na_2CO_3 addition to limestone inducing high-capacity SO_2 capture. Environ Sci Technol. 2017;51(21):12692–8. https://doi.org/10.1021/acs.est.7b04141.
24. Scala F, Chirone R, Meloni P, Carcangiu G, Manca M, Mulas G, et al. Fluidized bed desulfurization using lime obtained after slow calcination of limestone particles. Fuel. 2013;114:99–105. https://doi.org/10.1016/j.fuel.2012.11.072.

25. Anthony EJ, Bulewicz EM, Jia L. Reactivation of limestone sorbents in FBC for SO_2 capture. Prog Energy Combust Sci. 2007;33(2):171–210. https://doi.org/10.1016/j.pecs.2006.10.001.
26. Hu G, Dam-Johansen K, Wedel S, Hansen JP. Review of the direct sulfation reaction of limestone. Prog Energy Combust Sci. 2006;32(4):386–407. https://doi.org/10.1016/j.pecs.2006.03.001.
27. Bragança SR, Castellan JL. FBC desulfurization process using coal with low sulfur content, high oxidizing conditions and metamorphic limestones. Braz J Chem Eng. 2009;26(2):375–83. https://doi.org/10.1590/s0104-66322009000200015.
28. Lages VP, da Cunha ALC, Dweck J. Evaluation of SO_2 capture efficiency of combustion gases using commercial limestone. J Therm Anal Calorim. 2019;138(5):3833–43. https://doi.org/10.1007/s10973-019-08056-4.
29. Tarelho LAC, Matos MAA, Pereira FJMA. The influence of operational parameters on SO_2 removal by limestone during fluidised bed coal combustion. Fuel Process Technol. 2005;86(12):1385–401. https://doi.org/10.1016/j.fuproc.2005.03.002.
30. Obras-Loscertales MDL, Rufas A, de Diego LF, García-Labiano F, Gayán P, Abad A, et al. Morphological analysis of sulfated Ca-based sorbents under conditions corresponding to oxy-fuel fluidized bed combustion. Fuel. 2015;162:264–70. https://doi.org/10.1016/j.fuel.2015.09.016.
31. Wang C, Chen L, Jia L, Tan Y. Simultaneous calcination and sulfation of limestone in CFBB. Appl Energy. 2015;155:478–84. https://doi.org/10.1016/j.apenergy.2015.05.070.
32. Gullett BK, Bruce KR. Pore distribution changes of calcium-based sorbents reacting with sulfur dioxide. AIChE J. 1987;33(10):1719–26. https://doi.org/10.1002/aic.690331015.
33. Ghosh-Dastidar A, Mahuli S, Agnihotri R, Fan LS. Ultrafast calcination and sintering of $Ca(OH)_2$ powder: experimental and modeling. Chem Eng Sci. 1995;50(13):2029–40. https://doi.org/10.1016/0009-2509(95)00043-5.
34. Mahuli SK, Agnihotri R, Chauk S, Ghosh-Dastidar A, Wei SH, Fan LS. Pore-structure optimization of calcium carbonate for enhanced sulfation. AIChE J. 1997;43(9):2323–35. https://doi.org/10.1002/aic.690430917.
35. de Diego LF, Obras-Loscertales MDL, García-Labiano F, Rufas A, Abad A, Gayán P, et al. Characterization of a limestone in a batch fluidized bed reactor for sulfur retention under oxy-fuel operating conditions. Int J Greenhouse Gas Control. 2011;5(5):1190–8. https://doi.org/10.1016/j.ijggc.2011.05.032.
36. Fonseca AM, Órfão JJ, Salcedo RL. A new approach to the kinetic modeling of the reaction of gaseous HCl with solid lime at low temperatures. Chem Eng Sci. 2003;58(15):3499–506. https://doi.org/10.1016/S0009-2509(03)00219-7.
37. Maina P, Mbarawa M. Enhancement of lime reactivity by addition of diatomite. Fuel Process Technol. 2011;92(10):1910–9. https://doi.org/10.1016/j.fuproc.2011.05.011.
38. Cordero JM, Alonso M. Modelling of the kinetics of sulphation of CaO particles under CaL reactor conditions. Fuel. 2015;150:501–11. https://doi.org/10.1016/j.fuel.2015.02.075.
39. Liu H, Katagiri S, Kaneko U, Okazaki K. Sulfation behavior of limestone under high CO_2 concentration in O_2/CO_2 coal combustion. Fuel. 2000;79(8):945–53. https://doi.org/10.1016/S0016-2361(99)00212-4.
40. Qiu K, Lindqvist O. Direct sulfation of limestone at elevated pressures. Chem Eng Sci. 2000;55(16):3091–100. https://doi.org/10.1016/S0009-2509(99)00589-8.
41. Liu H, Katagiri S, Okazaki K. Drastic SO_x removal and influences of various factors in O_2/CO_2 pulverized coal combustion system. Energy Fuels. 2001;15(2):403–12. https://doi.org/10.1021/ef000171p.
42. Wang S, Zhao Y, Zhang P, Liu Y. Study of the sulfation kinetics between SO_2 and CaO catalyzed by TiO_2 nano-particles. Chem Eng Res Des. 2011;89(7):1061–6. https://doi.org/10.1016/j.cherd.2010.12.006.
43. Kim YB, Gwak YR, Keel SI, Yun JH, Lee SH. Direct desulfurization of limestones under oxy-circulating fluidized bed combustion conditions. Chem Eng J. 2019;377:119650. https://doi.org/10.1016/j.cej.2018.08.036.
44. Wu ZH, Kou P, Yu ZW. The modulation of desulphurization properties of calcium oxide by alkali carbonates. J Therm Anal Calorim. 2002;67(3):745–50. https://doi.org/10.1023/a:1014381510955.
45. Ar İ, Balci S. Sulfation reaction between SO_2 and limestone: application of deactivation model. Chem Eng Process. 2002;41(2):179–88. https://doi.org/10.1016/S0255-2701(01)00133-7.
46. Li Y, Sun R, Zhao J, Han K, Lu C. Sulfation behavior of white mud from paper manufacture as SO_2 sorbent at fluidized bed combustion temperatures. J Therm Anal Calorim. 2012;107(1):241–8. https://doi.org/10.1007/s10973-011-1537-2.
47. Yang JH, Shih SM. Preparation of high surface area $CaCO_3$ by bubbling CO_2 in aqueous suspensions of $Ca(OH)_2$: effects of $(NaPO_3)_6$, $Na_5P_3O_{10}$, and Na_3PO_4 additives. Powder Technol. 2010;197(3):230–4. https://doi.org/10.1016/j.powtec.2009.09.020.
48. Wang C, Zhang Y, Jia L, Tan Y. Effect of water vapor on the pore structure and sulfation of CaO. Fuel. 2014;130(130):60–5. https://doi.org/10.1016/j.fuel.2014.04.007.
49. Galloway BD, MacDonald RA, Padak B. Characterization of sulfur products on CaO at high temperatures for air and oxy-combustion. Int J Coal Geol. 2016;167:1–9. https://doi.org/10.1016/j.coal.2016.09.007.
50. Jeong S, Lee KS, Keel SI, Yun JH, Kim YJ, Kim SS. Mechanisms of direct and in-direct sulfation of limestone. Fuel. 2015;161:1–11. https://doi.org/10.1016/j.fuel.2015.08.034.
51. Han K, Lu C, Cheng S, Zhao G, Wang Y, Zhao J. Effect of characteristics of calcium-based sorbents on the sulfation kinetics. Fuel. 2005;84(14):1933–9. https://doi.org/10.1016/j.fuel.2005.04.001.
52. Li YR, Qi HY, You CF, Xu XC. Kinetic model of CaO/fly ash sorbent for flue gas desulphurization at moderate temperatures. Fuel. 2007;86(5):785–92. https://doi.org/10.1016/j.fuel.2006.09.011.
53. Wei F, Guo L, Liu Z, Shen X, Liu H. Thermogravimetric analysis of desulfurization characteristics and kinetic parameters of limestone modified by red mud. Adv Mater Res. 2012;512–515:2339–42. https://doi.org/10.4028/www.scientific.net/AMR.512-515.2339.
54. Chen H, Zhao Z, Huang X, Patchigolla K, Cotton A, Oakey J. Novel optimized process for utilization of CaO-based sorbent for capturing CO_2 and SO_2 sequentially. Energy Fuels. 2012;26(9):5596–603. https://doi.org/10.1021/ef300487q.
55. Hu G, Dam-Johansen K, Wedel S, Hansen JP. Direct sulfation of limestone. AIChE J. 2007;53(4):948–60. https://doi.org/10.1002/aic.11129.
56. Chen L, Wang C, Yan G, Zhao F, Anthony EJ. The simultaneous calcination/sulfation reaction of limestone under oxy-fuel CFB conditions. Fuel. 2019;237:812–22. https://doi.org/10.1016/j.fuel.2018.10.060.
57. Chen L, Wang Z, Wang C, Wang H, Anthony EJ. Sulfation of limestone under O_2/H_2O combustion conditions in circulating fluidized bed. Int J Greenh Gas Control. 2020;95:102979. https://doi.org/10.1016/j.ijggc.2020.102979.
58. Hu G, Dam-Johansen K, Wedel S, Hansen JP. Enhancement of the direct sulfation of limestone by alkali metal salts, calcium chloride, and hydrogen chloride. Ind Eng Chem Res. 2007;46(16):5295–303. https://doi.org/10.1021/ie070208u.
59. Cheng J, Zhou J, Liu J, Zhou Z, Huang Z, Cao X, et al. Sulfur removal at high temperature during coal combustion in furnaces:

a review. Prog Energy Combust Sci. 2003;29(5):381–405. https://doi.org/10.1016/S0360-1285(03)00030-3.
60. Chen C, Zhao C. Mechanism of highly efficient in-furnace desulfurization by limestone under O_2/CO_2 coal combustion atmosphere. Ind Eng Chem Res. 2006;45(14):5078–85. https://doi.org/10.1021/ie060196x.